

JUL 15 1958

UNCLASSIFIED

CONFIDENTIAL

Copy

3

RM A58C24

C-1

NACA RM A58C24

NACA

RESEARCH MEMORANDUM

INVESTIGATION OF THE PERFORMANCE AND INTERNAL FLOW OF

10-28-60
ERK
VARIABLE-AREA, VARIABLE-INTERNAL-CONTRACTION

INLET AT MACH NUMBERS OF 2.00, 2.50, AND 2.92

By Richard Scherrer and Warren E. Anderson

Ames Aeronautical Laboratory
Moffett Field, Calif.

FOR REFERENCE

LIBRARY COPY

JUL 16 1958

LANGLEY AERONAUTICAL LABORATORY
LIBRARY, NACA
LANGLEY FIELD, VIRGINIA

NOT TO BE REPRODUCED IN THIS ROOM

CLASSIFIED DOCUMENT

This material contains information affecting the National Defense of the United States within the meaning of the espionage laws, Title 18, U.S.C., Secs. 793 and 794, the transmission or revelation of which in any manner to an unauthorized person is prohibited by law.

NATIONAL ADVISORY COMMITTEE
FOR AERONAUTICS

WASHINGTON

July 15, 1958

CONFIDENTIAL

UNCLASSIFIED

CLASSIFICATION CHANGED

UNCLASSIFIED

To

By authority of



3 1176 01434 9584

CLASSIFIED

NATIONAL ADVISORY COMMITTEE FOR AERONAUTICS

RESEARCH MEMORANDUM

INVESTIGATION OF THE PERFORMANCE AND INTERNAL FLOW OF
A VARIABLE-AREA, VARIABLE-INTERNAL-CONTRACTION
INLET AT MACH NUMBERS OF 2.00, 2.50, AND 2.92*

By Richard Scherrer and Warren E. Anderson

SUMMARY

The performance of a variable-internal-contraction inlet without boundary-layer removal has been measured at Mach numbers of 2.00, 2.50, and 2.92. The total-pressure recovery at the design Mach number, 2.50, was 0.78. At Mach numbers 2.00 and 2.92 the maximum total-pressure ratios were 0.87 and 0.54, respectively. In general, the exit total-pressure ratio decreased with increasing exit flow unsteadiness, and attainment of steady exit static pressure appears to require a terminal-shock total-pressure ratio near unity.

INTRODUCTION

Internal-contraction inlets having variable capture area and variable contraction can in principle, provide high pressure recovery with low drag for Mach numbers above about 2.00 and ranges of altitude. Although internal-contraction inlets can have low external drag because of the small external slopes that can be employed, they generally have had greater internal wetted area than external-compression inlets. Therefore, the boundary layer represents a larger part of the flow at the terminal shock, and achievement of high pressure recovery is more difficult. Thus, the pressure-recovery problem in internal-contraction inlets appears to be one of minimizing internal boundary-layer growth and avoiding secondary flows.

Although boundary-layer control is an obvious solution to the problem of minimizing boundary-layer growth, it is not necessarily the only solution. It has not been included in the present investigation because the objective is to determine the improvements in internal performance that can be made by changes in the local pressure gradients. With such knowledge, further improvements should be possible with the minimum of boundary-layer control.

*Title, Unclassified

UNCLASSIFIED

In supersonic diffusion there is a marked difference between the theoretical longitudinal pressure distributions required for minimizing boundary-layer growth and those associated with efficient shock configurations. Minimum boundary-layer growth is obtained by employing the least length of unseparated flow, a fact which dictates the use of high initial and gradually decreasing pressure gradients in the flow direction. In contrast, efficient shock configurations require exactly the opposite pressure distributions, that is, low initial pressure gradients followed by steadily increasing gradients. These conflicting requirements cannot be resolved; however, in the contraction just ahead of the throat, the region of highest pressure gradient in multishock inlets, gradient reductions can be achieved with little over-all increase in duct length.

Numerous tests of internal-contraction inlets of several types have been reported (refs. 1, 2, 3, and 4) and the level of pressure recovery is gradually approaching that of external-compression inlets. The present experiments are intended to provide a basis for further improvements and are concerned with determining the effects on pressure recovery, flow uniformity, and steadiness of a series of changes in duct geometry. These changes include various initial compression surface angles, several cross-section area gradients in the throat region, and two shapes of subsonic diffuser. All of the changes affect the longitudinal static-pressure gradients in a rectangular inlet. Some of the design features recommended in reference 4 also have been incorporated in the present inlet. These include corner fillets which grow to a circular exit of the subsonic diffuser and small area gradients in the throat region. Since there is a lack of information about the details of the throat flow in internal-contraction inlets, the scope of the investigation included some study of the details of such flows.

Tests were conducted at Mach numbers of 2.00, 2.50, and 2.92 in the Ames 1- by 3-foot supersonic wind tunnel No. 2. The Reynolds numbers based on inlet width were constant at each Mach number and were 3.24 , 3.11 , and 2.98×10^6 at Mach numbers of 2.00, 2.50, and 2.92, respectively. The angle of attack was 0° .

SYMBOLS

Physical Symbols

A	duct cross-section area, sq in.
A_1	inlet area measured perpendicular to the duct center line at the flap leading edge, sq in.
M	Mach number

p	static pressure, lb/sq in.
p_t	total pressure, lb/sq in.
R	Reynolds number based on duct width
r	radius, in.
x	longitudinal distance from leading edge of side plate, in.
y	vertical distance from duct floor measured perpendicular to center line of the duct (see fig. 2(b)) in the duct center plane, in.
Y	duct height (measured as for y), in.
\bar{Y}_2	average throat height, minimum area/throat width, in.
z	lateral distance perpendicular to center line (see fig. 2(b))
Z	duct width, in.
δ_f	flap angle, deg

Subscripts

∞	free-stream conditions
1	inlet station located at the side-wall leading edge
2	minimum area station
3	diffuser exit station
min	minimum
max	maximum

Configuration Symbols

W_6	6° wedge insert
W_9	9° wedge insert
W_{12}	12° wedge insert

W_{9E} extended 9° wedge insert
 F_6 6° fillet insert
 f_2 2-inch-long flexure
 f_5 5-inch-long flexure
 D_3 3° wall angle diffuser
 D_5 5° wall angle diffuser

APPARATUS

Wind Tunnel

The experiments were conducted in the Ames 1- by 3-foot supersonic wind tunnel No. 2. This wind tunnel is of the intermittent-operation, nonreturn, variable-pressure type and is equipped with a nozzle having flexible top and bottom plates for varying the test Mach number. Tests were conducted at Mach numbers of 2.00, 2.50, and 2.92 at Reynolds numbers, based on inlet width, of 3.24×10^6 , 3.11×10^6 , and 2.98×10^6 , respectively. The model was mounted from a rigid support strut that spanned the wind tunnel downstream of the test section.

Model

A photograph of the model is shown in figure 1, and a drawing of the basic model showing several cross sections is shown in figure 2. The model has a rectangular entrance and has both adjustable throat height and variable forward flap angle. The cross-sectional shape differs from rectangular in that the corners are filleted and the fillets increase in size in the flow direction. The fillets merge at the diffuser exit to form a nearly circular duct. The length of the inlet from the leading edge to the throat was selected for near-optimum three-shock pressure recovery at a Mach number of 2.5 with the duct floor parallel to the free-stream direction and with the throat height set at the 3-inch position.

The nominal throat location is at the 13.87-inch station and the bottom and sides of the duct each diverge at an angle of 1° from the center line at this station. This region of 1° divergence extends to the 17.87-inch station where the subsonic diffuser is considered to begin. The original subsonic diffuser for a 3-inch throat height had an area ratio equivalent to that of a 6° conical diffuser of equal length. This diffuser design at the 2.5-inch throat height resulted in local wall

angles of nearly 6° in the vertical center plane of the inlet and angles of less than 3° on the side walls. The maximum local divergence angle was reduced, after initial tests, to 3° for the 2.5-inch throat height. As a result of the subsonic diffuser revision the circular duct exit was changed as shown in figure 2.

The series of wedge inserts for the supersonic flow region, which are listed under configuration symbols, were designed to provide additional compression waves, to cancel partially the bow shock from the movable flap, and to reduce the rate of contraction in cross-section area between the crest of the insert and the throat. The fillet insert F_8 has the same axial distribution of cross-section area as the 6° wedge insert and was included to illustrate the effect of three-dimensional shocks and less wetted area. The extended wedge insert, W_{8E} , was included to provide a more smooth cross-sectional area distribution in the throat region. The dimensions of the inserts are given in the drawings of figure 3. Sample longitudinal distributions of cross-section area are given in figure 4, and the typical insert position in the duct is shown in figure 5. It should be noted in figure 4 that with the inserts in the duct the throat position and area vary with flap angle. In the discussion of the results, the W_8 , W_9 , W_{12} , and F_8 inserts will be mentioned collectively as short inserts while the W_{8E} insert is mentioned as the extended or long insert.

Two flexure plates were tested: one 2 inches long and the other 5 inches long. The purpose of these flexures was to determine the effect of two variations in rate of contraction in addition to the variations in rate of contraction provided by the inserts. The structural details of this flexure are shown in figure 5, and typical throat area distributions are given in figure 4. The throat height with the short flexure was adjustable in $1/2$ -inch increments between about 2.5 and 4 inches. With the long flexure the throat heights without inserts were 2.26, 2.76, and 3.26 inches. Use of the 5-inch flexure, relative to the 2-inch flexure, allowed somewhat larger flap angles for a given contraction ratio and also caused larger changes in throat area and position with flap angle.

Instrumentation

The instrumentation in the model of the present investigation consisted of the following items:

1. Exit total- and static-pressure rake (see fig. 2)
2. Static-pressure orifices along the center line of the duct wall
3. Throat boundary-layer rakes, one on the duct floor with the tube tips at station 17 and another on the side wall at station 16

4. Two static-pressure transducers, one on the side wall at station 17 and the other near the exit rake (see fig. 2(a))
5. Angle-of-attack transducer, of the damped pendulum type, for indicating flap angle

All of the pressures were recorded by photographing mercury-in-glass manometers. With this pressure-measurement apparatus the average total-pressure ratio measurements are accurate to within $\pm 0.005 p_{t_\infty}$. Calibration of the flap-angle transducer system indicated a maximum error of 0.1° at any angle. The static-pressure transducers were used to indicate the flow unsteadiness near the throat and at the rake stations and could have a maximum absolute error as great as 10 percent of the instantaneous static-pressure fluctuation. This was not considered unreasonable because the primary purpose of the transducers was to indicate the presence of unsteady flow.

All of the total-pressure ratios are presented as area average values except that shown to compare the subsonic diffusers. Because structural failure of the exit rake occurred during tests with the D_5 diffuser, the total-pressure ratios presented from these tests are mass derived values (see ref. 5).

Total- and static-pressure measurements made with manometers do not indicate such important information as shock-wave motions or transient exit flow distortions because manometers have poor frequency response. Thus, it is essential that pressure instrumentation with adequate frequency response be employed in air-induction system tests, if all sources of pressure loss are to be indicated. Insofar as the present experiments are concerned, the manometer pressure measurements are subject to unknown inaccuracies which are dependent upon the peak-to-peak amplitude and frequency of occurrence of the static-pressure oscillations. For the minimum values of static-pressure unsteadiness, the errors in mean pressures are believed to be negligible because the relative duration of the maximum amplitude disturbances was small.

TESTS

At each Mach number, tests were conducted with several duct configurations for several throat heights, flap angles, and terminal shock positions. All configurations were tested at Mach number 2.50. The tests at Mach numbers 2.00 and 2.92, however, were exploratory in nature and did not include all configurations. The test procedure employed was nearly identical to that discussed in reference 4 for a similar variable inlet, the major difference being in the provision of an adjustable rather than remotely controlled throat height.

The test program was divided into three parts: (1) a brief study of the subsonic diffusers, (2) tests of five inserts, and (3) tests of selected inserts with the long throat flexure. It was found in the first tests that there was extensive separation in the D_5 diffuser. This was probably due to the large local wall angles resulting from the shape transition from the rectangular throat to the circular exit. The maximum wall angles were then reduced to 3° and the tests completed with this, D_3 , configuration.

RESULTS AND DISCUSSION

Total-Pressure Recovery and Contraction Ratio

The test data for total-pressure recovery, p_{t_3}/p_{t_∞} , and contraction ratio, A_1/A_{min} , have been presented together in figures 6 to 11 because the contraction ratio is an indication of the supersonic pressure recovery. This method of presentation allows a qualitative evaluation of the relative pressure losses in the supersonic and subsonic portions of the flow. The data are plotted as functions of the average throat height, \bar{Y}_2 , and the data points shown are only those for the maximum contraction ratio for each throat height.

Subsonic diffuser, $M_\infty = 2.50$ (fig. 6).- The effect of changing the configuration from that having a maximum local diffuser wall angle of over 5° , D_5f_2 , to one having a maximum angle of 3° , D_3f_2 , was to increase the total-pressure recovery by 0.06. Further increase resulted from adding the 6° wedge insert, W_3 , the total increase in recovery being 0.15. The diffuser change resulted in some reduction in maximum contraction ratio. This indicates that it was possible for the downstream flow to affect the flow in the throat because the upstream duct contours were unchanged.

Comparison of short inserts, $M_\infty = 2.50$ (fig. 7).- The pressure recovery improved with decreasing throat heights for all inserts. This was due to the greater number of shocks that occurred because of the increased ratio of supersonic flow length to throat height. The various inserts provided different contraction ratios at best pressure recovery, and there was little difference in the best total-pressure ratios for the various inserts. Since contraction ratio is an indication of total-pressure recovery up to the throat, it appears that the subsonic diffuser efficiency changed with the changes in inserts.

Comparison of long and short flexures, $M_\infty = 2.50$ (fig. 8).- The most marked effect of flexure length was on the contraction ratios and pressure recovery of the 6° insert configurations. The pressure recovery of the 9° insert configuration was improved slightly but with a slight

decrease in maximum contraction ratio. In general, it appears that the long flexure provided marked improvements in pressure recovery for the poorest configurations and only slight improvements in the best configuration.

Effect of the extended insert, $M_\infty = 2.50$ (fig. 9).- The effect of the extended insert used with the long flexure was to increase the pressure recovery and contraction slightly at the greater throat heights. The short flexure with the long insert resulted in little change in contraction ratio; however, marked reduction in total-pressure ratio occurred. The effect of removing the two flow survey rakes from the throat was an increase in pressure ratio of 0.02 which resulted in a maximum total-pressure ratio of 0.78. Although the increase in pressure ratio was only measured with the extended insert in the long flexure configuration, it is not unlikely that a comparable improvement would have been measured for all other configurations.

Comparison of short inserts, $M_\infty = 2.00$ (fig. 10).- The effect of throat height on total-pressure ratio at $M_\infty = 2.00$ is opposite to that at 2.50 and the effect on contraction is markedly less than at $M_\infty = 2.50$. The pressure recovery was best for the 6° wedge insert at the higher throat heights, probably as a result of the low subsonic diffuser angle which was 0° to 1° when the throat was near the crest of the insert. The 9° wedge insert provided the best contraction, but had a larger subsonic diffuser angle downstream of the crest of the insert. It might be expected that the extended 9° insert, which was not tested at a Mach number of 2.00, could have been superior to the 9° insert because the extension provided a smaller subsonic diffuser angle downstream of the crest of the insert. The long flexure was not tested at a Mach number of 2.00, but it is felt that the effect would have been small for the best configurations because the flexure was in a subsonic flow region with a small divergence angle at this Mach number.

Comparison of inserts and flexures, $M_\infty = 2.92$ (fig. 11).- The largest contraction ratio was obtained with the 9° extended wedge insert, and the maximum pressure recovery was also obtained with this configuration. It is apparent at this Mach number that the long flexure configuration was superior to the short one. The rapid improvement in pressure recovery with reducing throat height was due to the increasing ratio of supersonic flow length to throat height and the resulting increase in the number of oblique shocks. Further improvement in pressure recovery is to be expected for an inlet having a greater ratio of supersonic flow length to throat height.

Flow Unsteadiness and Distortion

Flow parameters.- Two parameters are used to describe the flow distortion at the diffuser exit. The distortion is described by

representative values for both radial and circumferential distortion. Radial distortion is the maximum difference in total pressure existing on any one of the six radial arms of the exit rakes, and this difference is divided by the area average total pressure to obtain a dimensionless parameter. Similarly, the circumferential distortion is taken as the maximum difference in total pressure occurring at the two-thirds radius on the six arms of the exit rake. This radial location for measuring distortion was found to give a maximum value for the present tests.

The flow unsteadiness parameter shown in figures 12 to 16 is based on the difference between the maximum and minimum pressures as obtained from photographs of oscilloscope traces of the static-pressure transducer outputs. It will be seen that the peak-to-peak pressure fluctuations were large for all configurations tested. For wave forms having occasional peaks, such as observed in the present investigation, the more commonly used mean values are small fractions of the peak-to-peak value. The choice of parameter in the present investigation was made to emphasize the fact that occasional large amplitude disturbances occur in internal flow systems.

Comparison of short inserts, $M_{\infty} = 2.50$ (fig. 12).- In general, the radial distortions at the exit were greater than the circumferential distortions which indicates large boundary-layer growth along the duct. The inserts reduced both the radial and circumferential distortions and thus must have reduced boundary-layer growth. The higher pressure recovery that occurred at small throat heights was coincident with lowest measured values of distortion and unsteadiness. The least unsteadiness for the wedge inserts was from 10 to 20 percent of the exit total pressure, which is considered to be large, and leads one to suspect that the distortion patterns were also time dependent.

Comparison of long and short flexures, $M_{\infty} = 2.50$ (fig. 13).- Although the long flexure improved the pressure recovery (fig. 8), it is apparent in figure 13 that the long flexure caused some increase in exit distortion and unsteadiness. However, the increase in distortion for the best pressure-recovery insert, W_9 , was not large. As will be shown later, the flow uniformity near the throat was increased by the change from the $D_{3f2}W_9$ to the $D_{3f5}W_9$ configuration.

Effect of the extended insert, $M_{\infty} = 2.50$ (fig. 14).- The extended 90° insert had little effect on exit distortion relative to the short 90° insert, and flow unsteadiness with the extended insert configuration $D_{3f5}W_{9E}$ was increased somewhat at the maximum contraction (minimum \bar{V}_2) from that shown in figure 13 for the $D_{3f2}W_9$ configuration.

Comparison of inserts and flexures, $M_{\infty} = 2.00$ (fig. 15).- The flow unsteadiness and circumferential distortion were reduced at $M_{\infty} = 2.00$ relative to $M_{\infty} = 2.50$ (see fig. 12); however, the radial distortion

still indicated large boundary-layer growth. This was unexpected because it was felt that the geometric asymmetry, which moved the throat forward with decreasing Mach number, would result in less boundary-layer growth and therefore less distortion.

Comparison of inserts and flexures, $M_\infty = 2.92$ (fig. 16).— The configurations that provided the best pressure recovery at $M_\infty = 2.92$, $D_{3f5W_{9E}}$, also provided the best exit flow; however, peak unsteadiness values as great as 30 percent of exit total pressure existed in this flow.

Flow Distortion at Station 17, $M_\infty = 2.50$

Total-pressure profiles at station 17 for three configurations having the best pressure recovery at the exit are shown in figure 17. Longitudinal static-pressure distributions for the same test conditions as the data of figure 17 are shown in figure 18 to illustrate further the nature of the transonic flow. The profiles in figure 17 indicate a thin side-wall boundary layer and a thick boundary layer on the floor of the duct. It should be noted that the relative locations of the outer end tubes in the total-pressure rakes as shown in figure 2(b) allow plotting of the pressure measured at $z/Z = 0.32$ and $y/Y \sim 0.75$ as well as at $z/Z = (1.0 - 0.32)$ and $y/Y \sim 0.75$ to provide a rough check on the uniformity of the flow. Dashed lines are used to indicate the extension of each data curve from the vertical rake to the data point from the horizontal rake. It appears from figures 17 and 18 that for the configuration with the most constant wall static pressure upstream of the throat, $D_{3f5W_{9E}}$, the flow is most uniform. The flow is less uniform for the D_{3f5W_9} configuration, and still less uniform for the configuration having the most rapid contraction to the throat, D_{3f2W_9} .

The tabulated values of total-pressure ratio in figure 17 indicate that the expected favorable effect of the gradually decreasing contraction rate ahead of the throat was not realized as an increase in exit total-pressure ratio relative to that with rapid contraction. This is believed to be related to the somewhat greater exit flow unsteadiness of $D_{3f5W_{9E}}$ that can be seen by comparison of the data for the D_{3f2W_9} configuration in figure 13 with that for $D_{3f5W_{9E}}$ in figure 14. Such a decrease in pressure recovery with increasing unsteadiness is also indicated by the data of reference 6 and by an over-all correlation of the data of this investigation which is presented in the next section.

Summary Data Correlations

Total-pressure ratio and contraction ratio, (fig. 19).- All of the test data from the present investigation are plotted in figure 19, against the ratio of measured contraction ratio to isentropic contraction ratio, to allow a comparison with one-dimensional flow theory. Two theoretical lines are shown in the figure, one for an adiabatic contraction to a throat Mach number of 1.0 and the other for adiabatic contraction to a throat Mach number of 1.6. The theoretical lines represent the total-pressure ratio up to the throat minus normal shock loss and minus an estimated 4-percent total-pressure loss in the subsonic diffuser. Thus, the theoretical lines are qualitatively comparable with the experimental data.

The theory and the test data indicate an increase in total-pressure recovery with increasing contraction ratio. Although the data at the highest test Mach number agree with the general trend, the level of these data points is markedly below that of the theory. Two data points obtained at $M = 2.50$ also lie at a lower level of pressure recovery. These two data points were obtained with the configuration having the D_5 subsonic diffuser. Since the theoretical recovery, at constant percent of isentropic contraction, increases with increasing throat Mach number, M_2 , the low values of total pressure that were measured must be due to losses in addition to that estimated for the normal shock and subsonic diffuser. The most obvious additional loss is that due to shock-wave boundary-layer interaction at the terminal shock and the effect of the resultant flow on the subsonic diffuser efficiency. The fact that the change of diffuser from D_5 to D_3 , at $M = 2.50$, reduces the losses substantially at a nearly fixed contraction can be construed as indicating that the diffuser efficiency is sensitive to local divergence angle for the particular in-flow conditions of the present experiments.

At a Mach number of 2.50 the test data lie along a line extending upward from the theoretical line for $M_2 = 1.6$ toward that for $M_2 = 1.0$. This trend demonstrates that both theory and experiment demand throat Mach numbers near unity for the large percentages of isentropic contraction that are required for high total-pressure ratios.

At a Mach number of 2.00 the throat Mach number was less than 1.6; in fact, for the highest contraction it was calculated that the throat Mach number was less than 1.4. The data for each configuration at Mach number 2.00 do not have any consistent trend relative to the theoretical lines, and the differences between the flow in each configuration cannot be isolated.

Total-pressure ratio and unsteadiness (fig. 20).- All of the exit flow unsteadiness data obtained in the present investigation are shown in figure 20. The data have been plotted against total-pressure ratio to

determine if any correlation exists. It is apparent that there is an increase in unsteadiness with increasing Mach number and decreasing total-pressure ratio. At each Mach number there is no clear trend in the variation of unsteadiness with total-pressure ratio.

Terminal-shock static-pressure ratio (fig. 21).- Examination of the longitudinal static-pressure distributions showed that the terminal shock was particularly well defined when shock pressure rise was smallest. It was concluded that the shock oscillations for this condition must have been small and thus it would be reasonable to correlate flow unsteadiness with shock pressure ratio. The correlation is shown in figure 21 for those tests having well-defined terminal shocks. The data indicate a decrease in unsteadiness with decreasing terminal-shock pressure ratio, and it appears that to attain steady exit flow the terminal-shock pressure ratio must be near 1.0.

CONCLUSIONS

The results of the investigation support the following conclusions:

1. The peak total-pressure recovery at the exit is 0.87, 0.78, and 0.54 at Mach numbers of 2.00, 2.50, and 2.92, respectively.
2. The peak-to-peak exit static-pressure unsteadiness at Mach number 2.50 was from 10 to 15 percent of the exit total pressure for the configurations having the best total-pressure recovery.
3. Attainment of steady exit flow appears to require a terminal-shock total-pressure ratio near unity.
4. The effect on pressure recovery and steadiness of reducing rates of contraction in the flow direction ahead of the throat was not clearly defined.

Ames Aeronautical Laboratory
National Advisory Committee for Aeronautics
Moffett Field, Calif., Mar. 24, 1958

REFERENCES

1. Mossman, Emmet A., and Pfyl, Frank A.: An Experimental Investigation at Mach Numbers From 2.1 to 3.0 of Circular-Internal-Contraction Inlets With Translating Centerbodies. NACA RM A56G06, 1956.

2. Gunther, Fred L.: Development of a Two-Dimensional Adjustable Supersonic Inlet. C.I.T., JPL Progress Rep. 20-247, Nov. 20, 1954.
3. McLafferty, G. H., Krasnoff, E. L., Ranard, E. D., Rose, W. G., and Vergara, R. D.: Investigation of Turbojet Inlet Design Parameters. Res. Dept. Rep. R-0790-13, United Aircraft Corp., Dec. 1955.
4. Scherrer, Richard, and Gowen, Forrest E.: Preliminary Experimental Investigation of a Variable-Area, Variable-Internal-Contraction Air Inlet at Mach Numbers Between 1.42 and 2.44. NACA RM A55F23, 1955.
5. Davis, Wallace F., and Scherrer, Richard: Aerodynamic Principles for the Design of Jet-Engine Induction Systems. NACA RM A55F16, 1956.
6. Scherrer, Richard, and Anderson, Warren E.: Preliminary Investigation of a Family of Diffusers Designed for Near Sonic Inlet Velocities. NACA TN 3668, 1956.

~~CONFIDENTIAL~~

NACA RM A58C24

~~CONFIDENTIAL~~

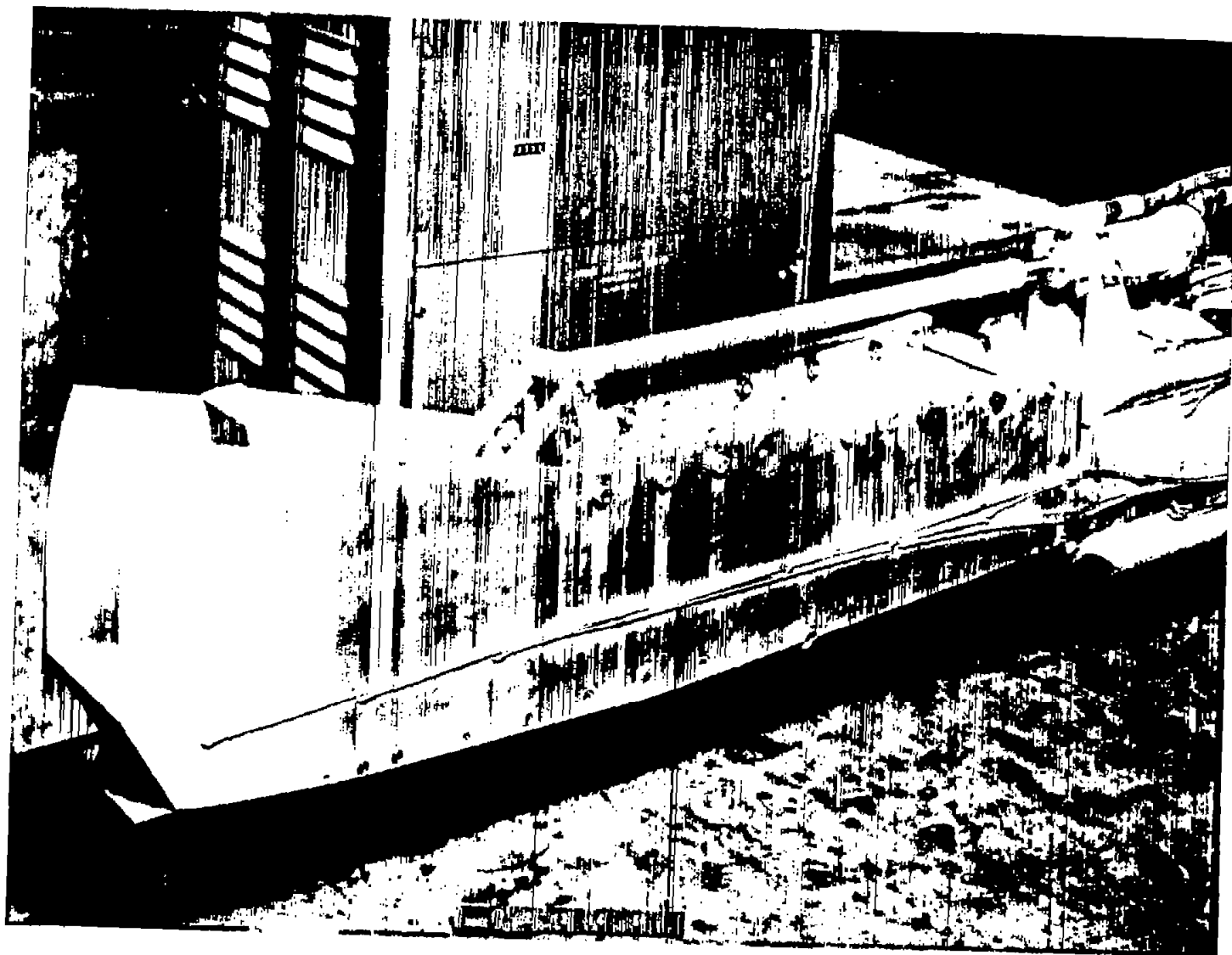
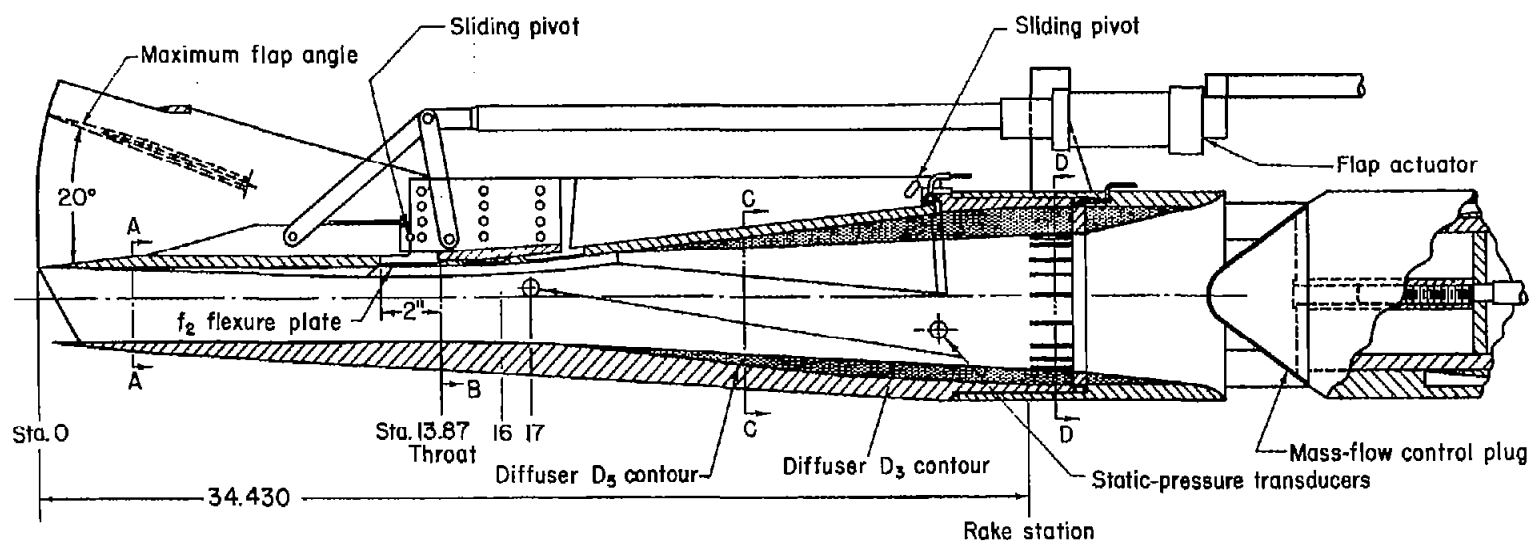


Figure 1.- Rectangular variable-internal-contraction inlet.

A-20724



(a) Vertical cross section through the longitudinal axis.

Figure 2.- Details of the D_3f_2 and D_5f_2 configurations.



Figure 2.- Concluded.

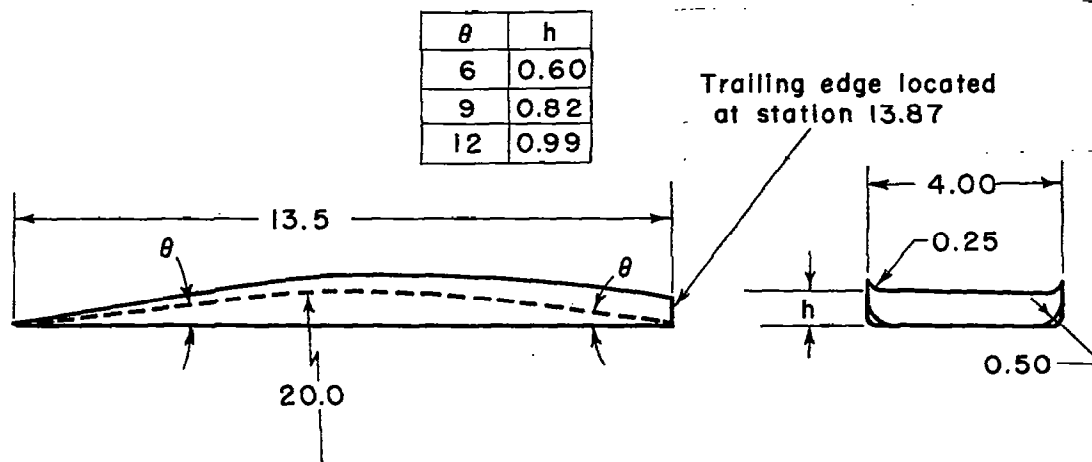
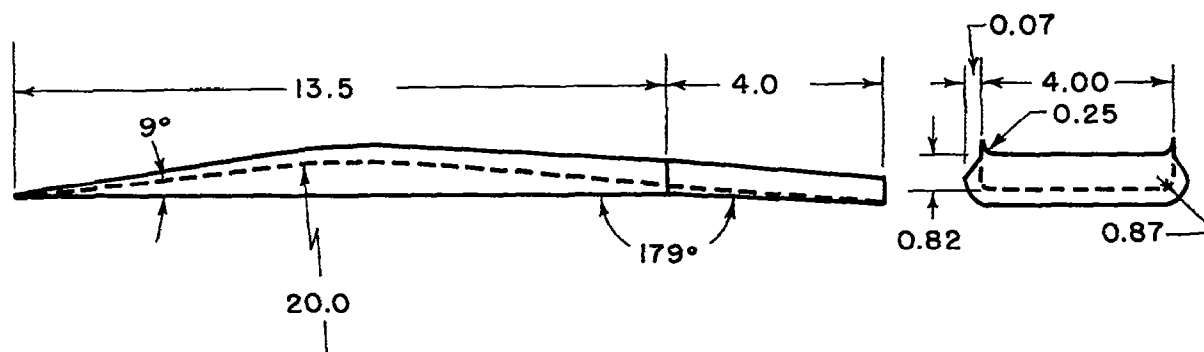
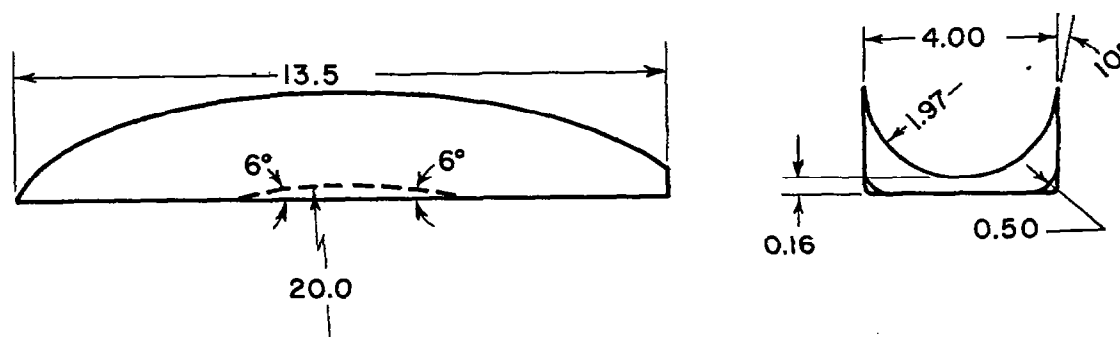
(a) Wedge inserts W_6 , W_9 and W_{12} .(b) Wedge insert W_{9E} (c) Fillet insert F_6 .

Figure 3.- Insert details.

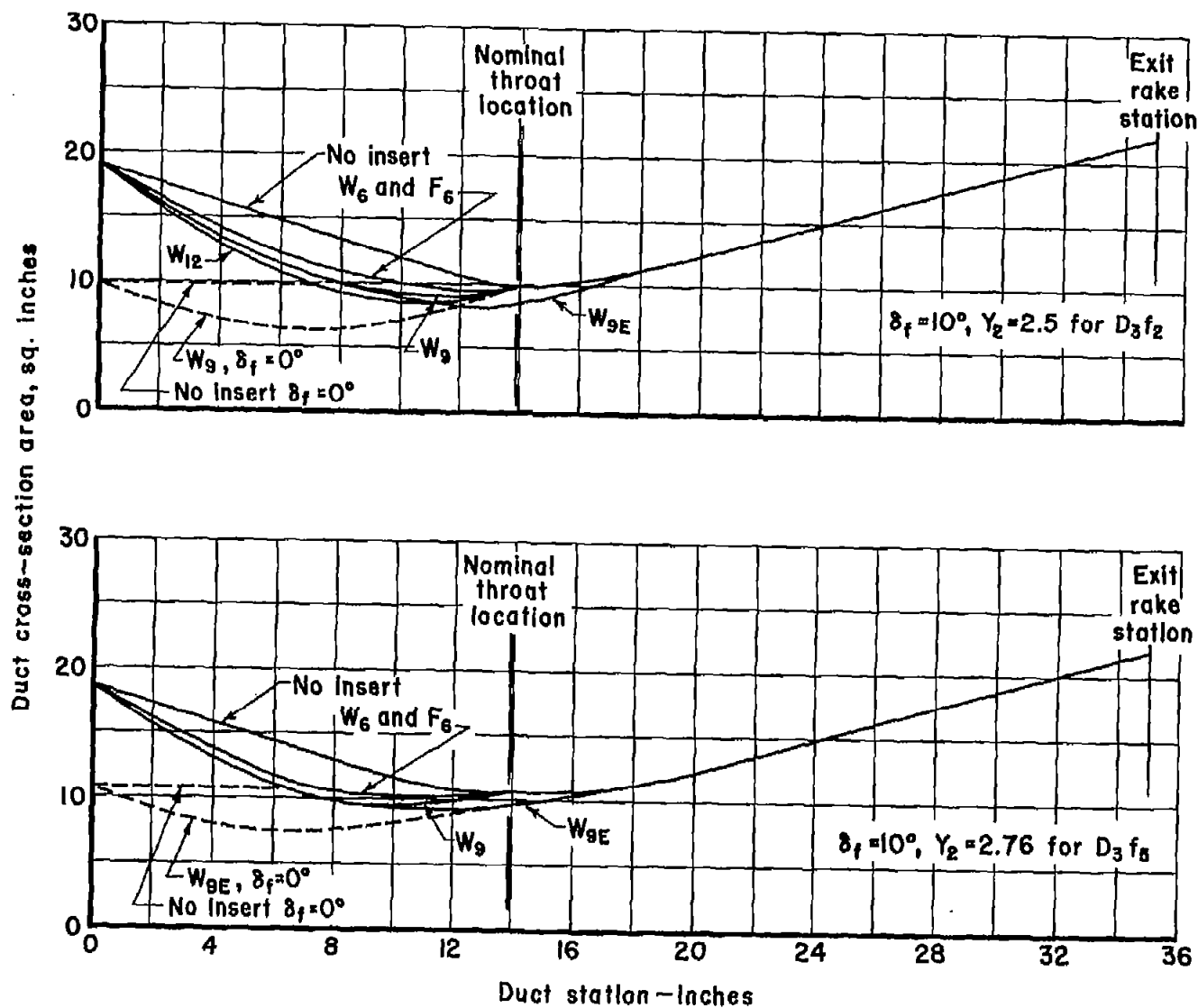


Figure 4.- Typical cross-sectional area distributions.

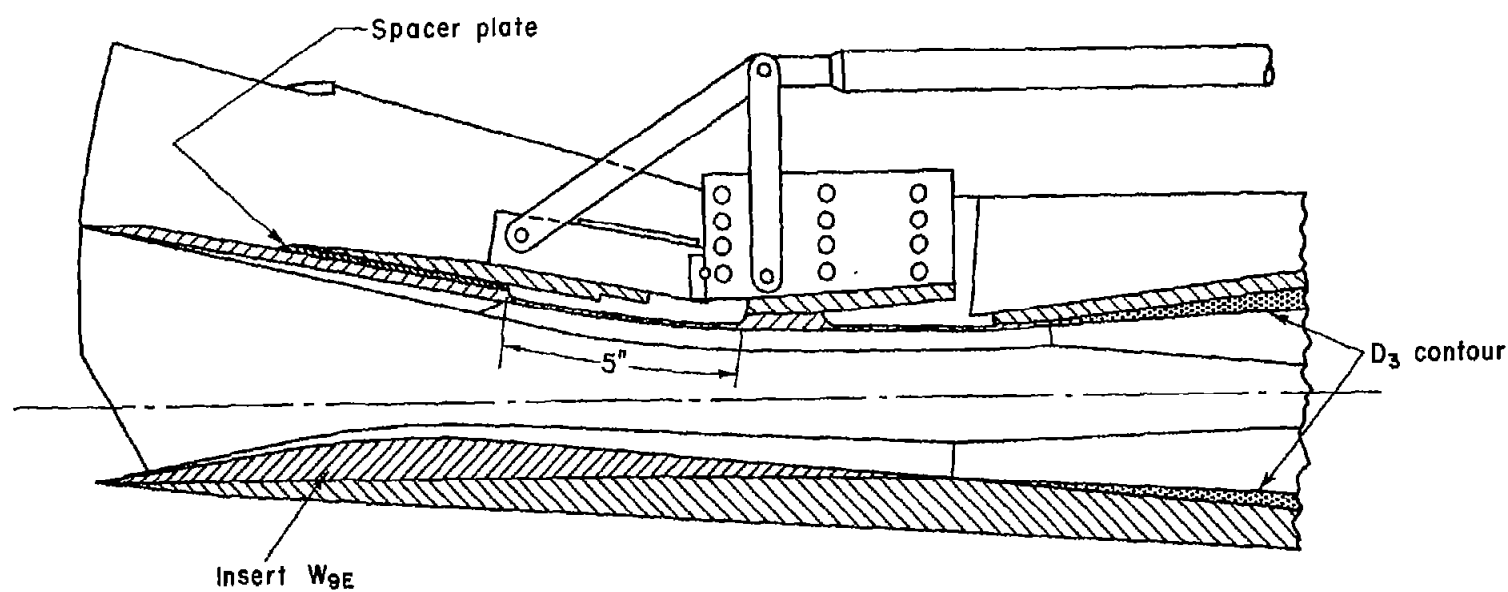


Figure 5.- Details of configuration $D_{35}^f W_{9E}$ at a flap angle of 10° .

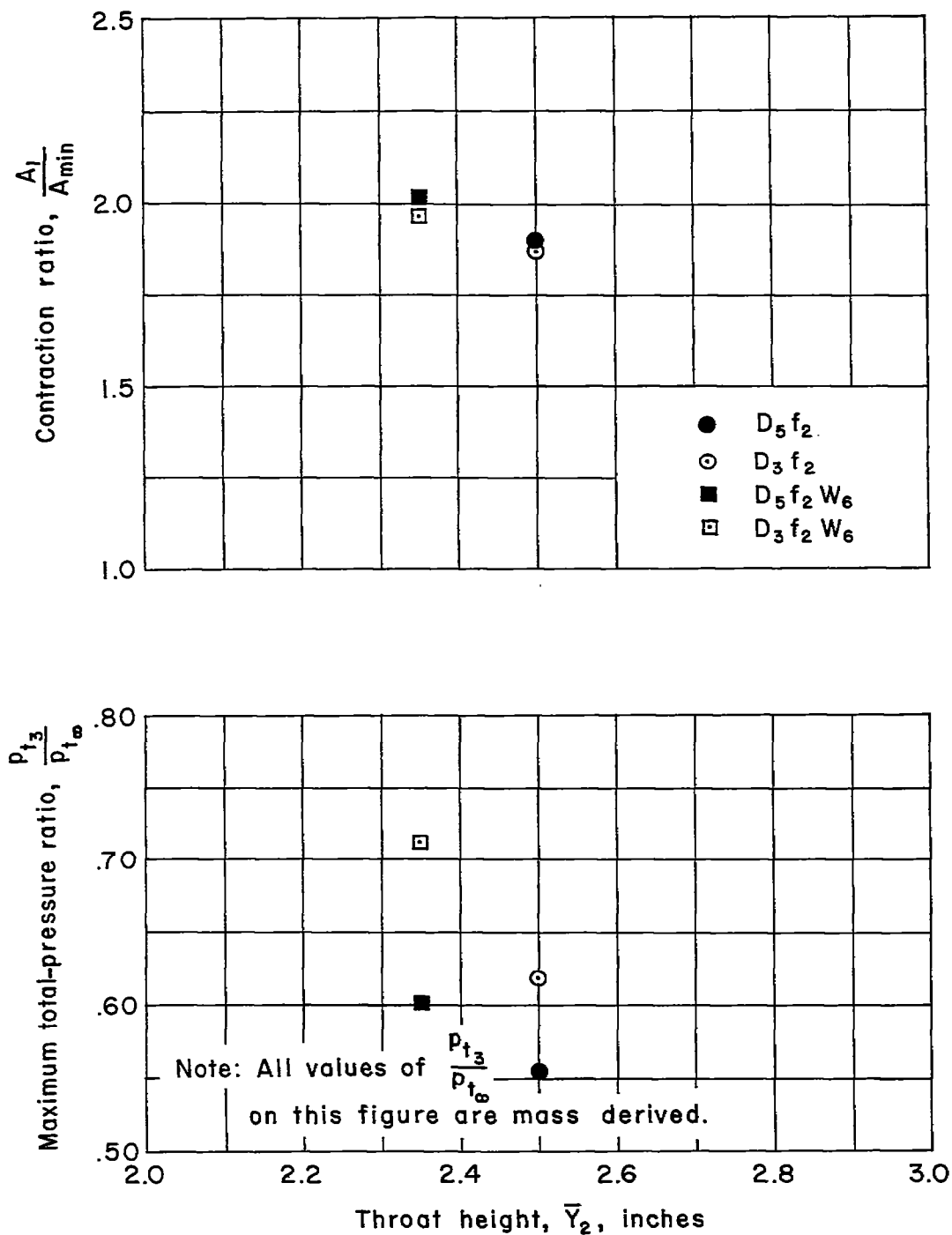


Figure 6.- Effect of changing the maximum local wall angle in the subsonic diffuser; $M_\infty = 2.50$.

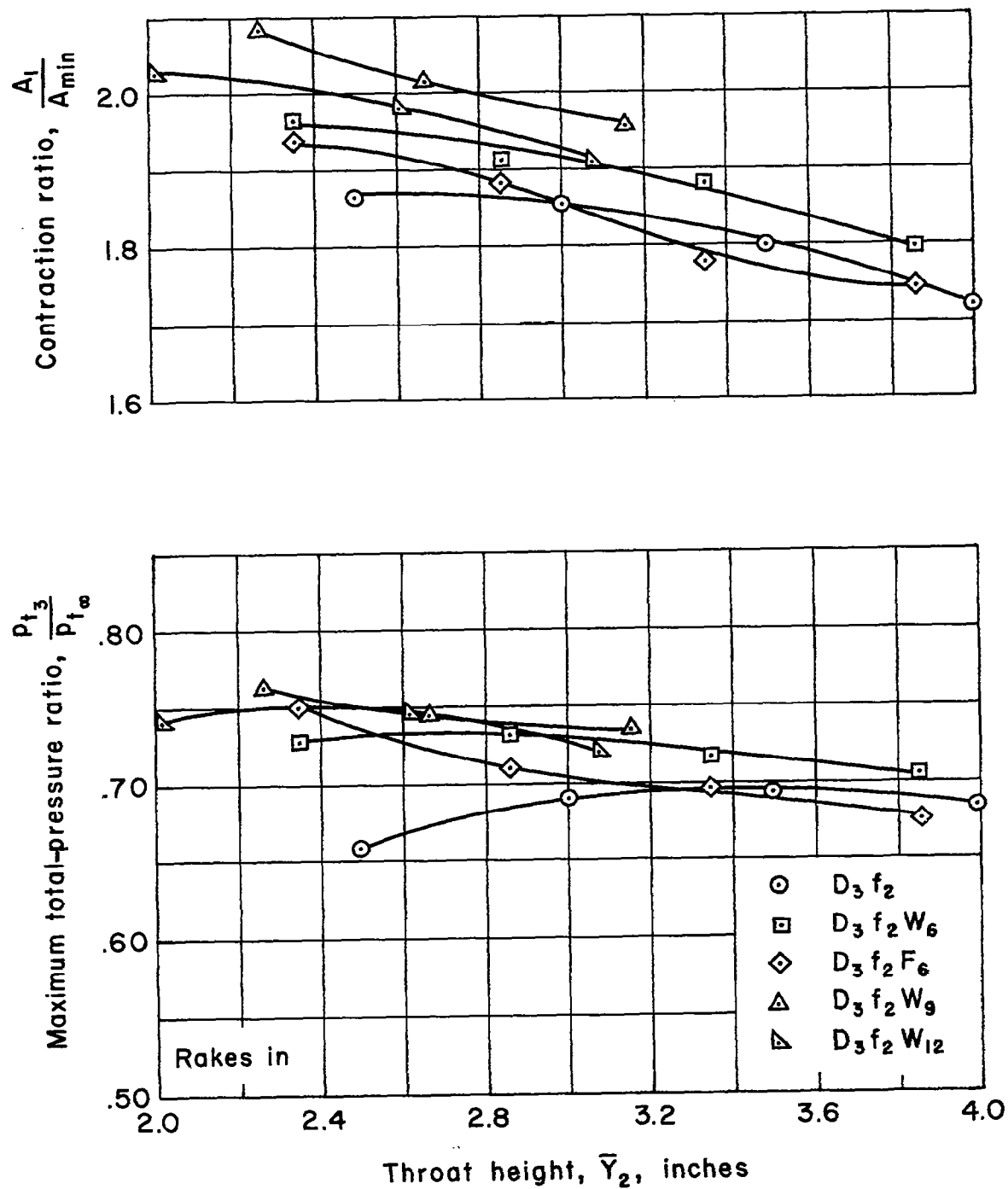


Figure 7.- Comparison of the total-pressure ratio and contraction ratios of the short inserts with the short flexure at $M_\infty = 2.50$.

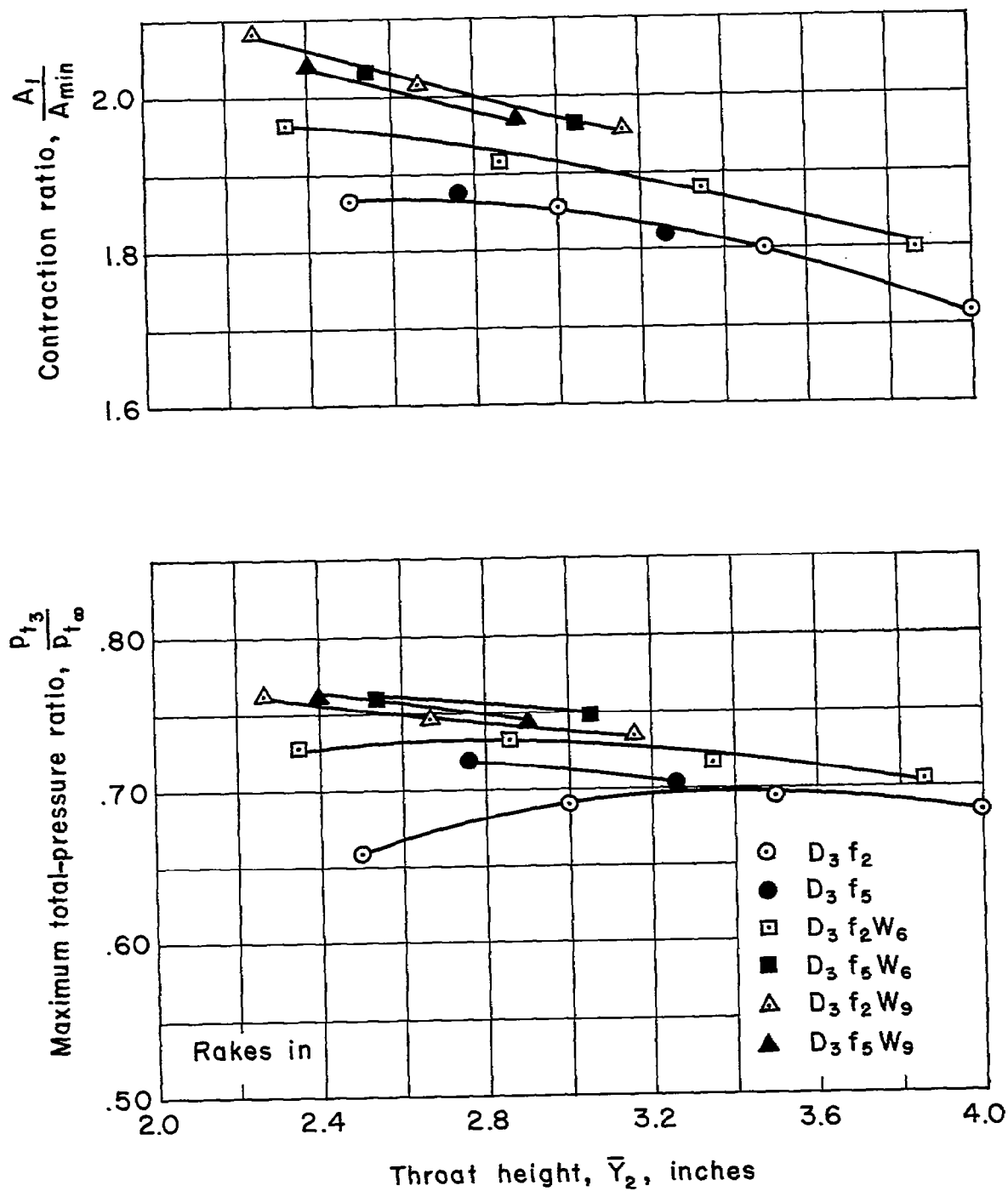


Figure 8.- Comparison of the total-pressure ratio and contraction ratios of the long and short flexure configurations with several inserts at $M_\infty = 2.50$.

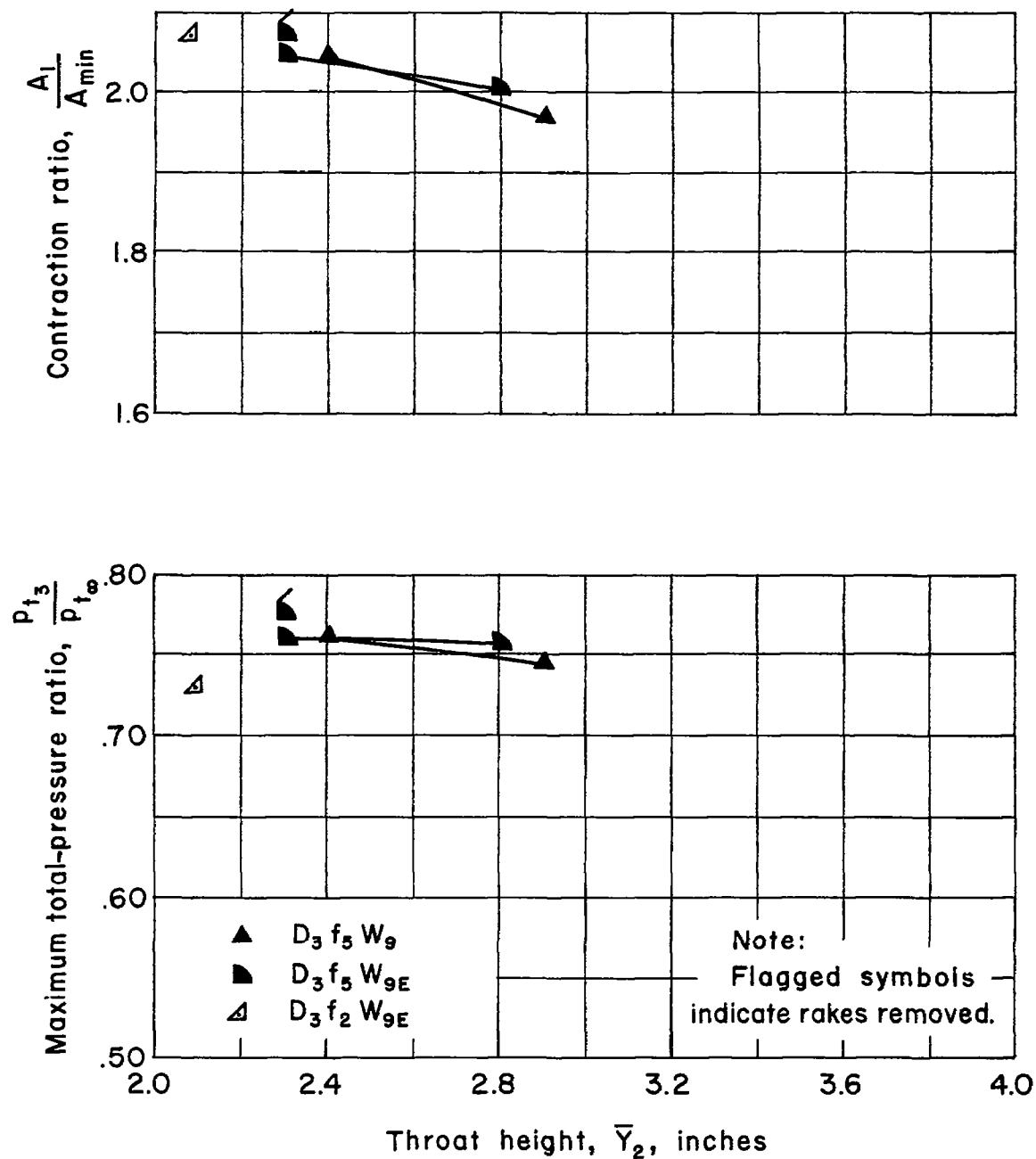


Figure 9.- Comparison of the total-pressure ratio and contraction ratios of the short and extended 9° inserts at $M_\infty = 2.50$.

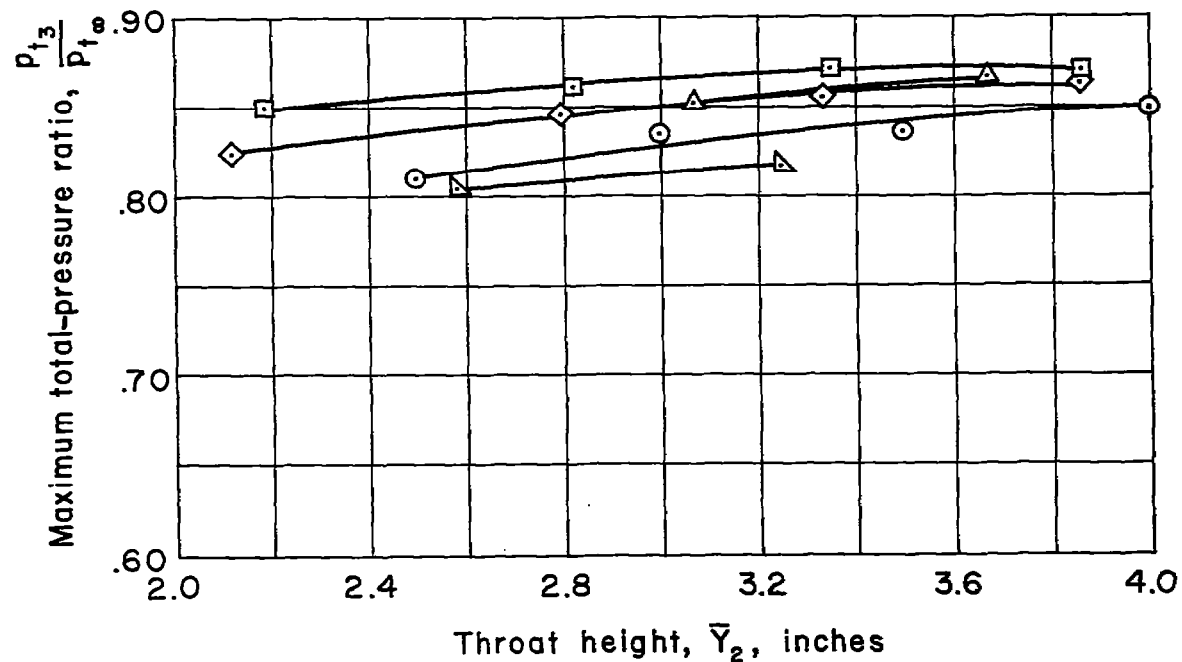
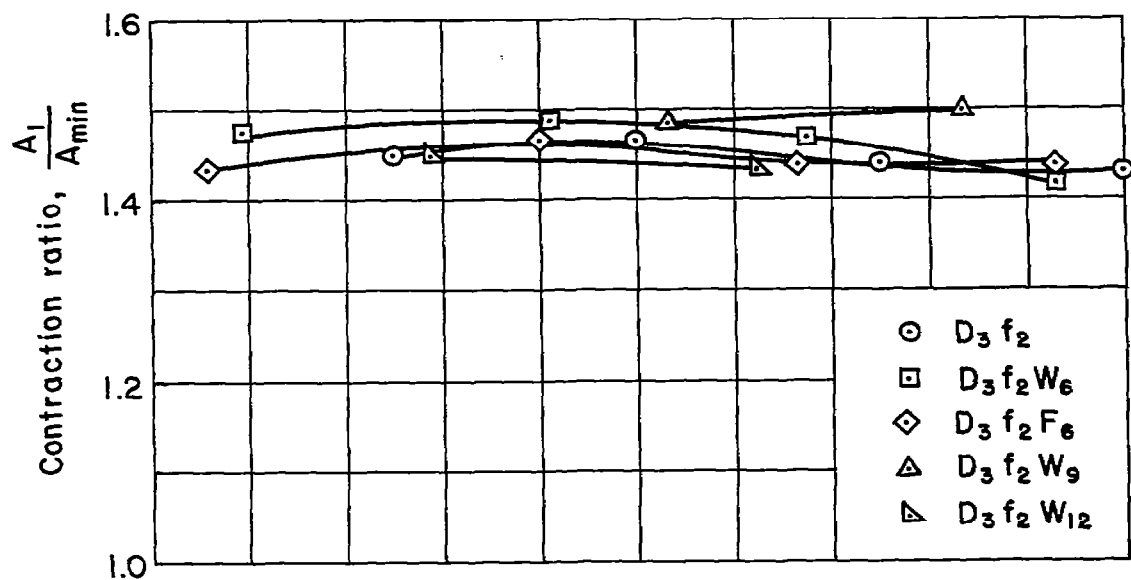


Figure 10.- Comparison of the total-pressure ratio and contraction ratios of the short inserts with the short flexure at $M_\infty = 2.00$.

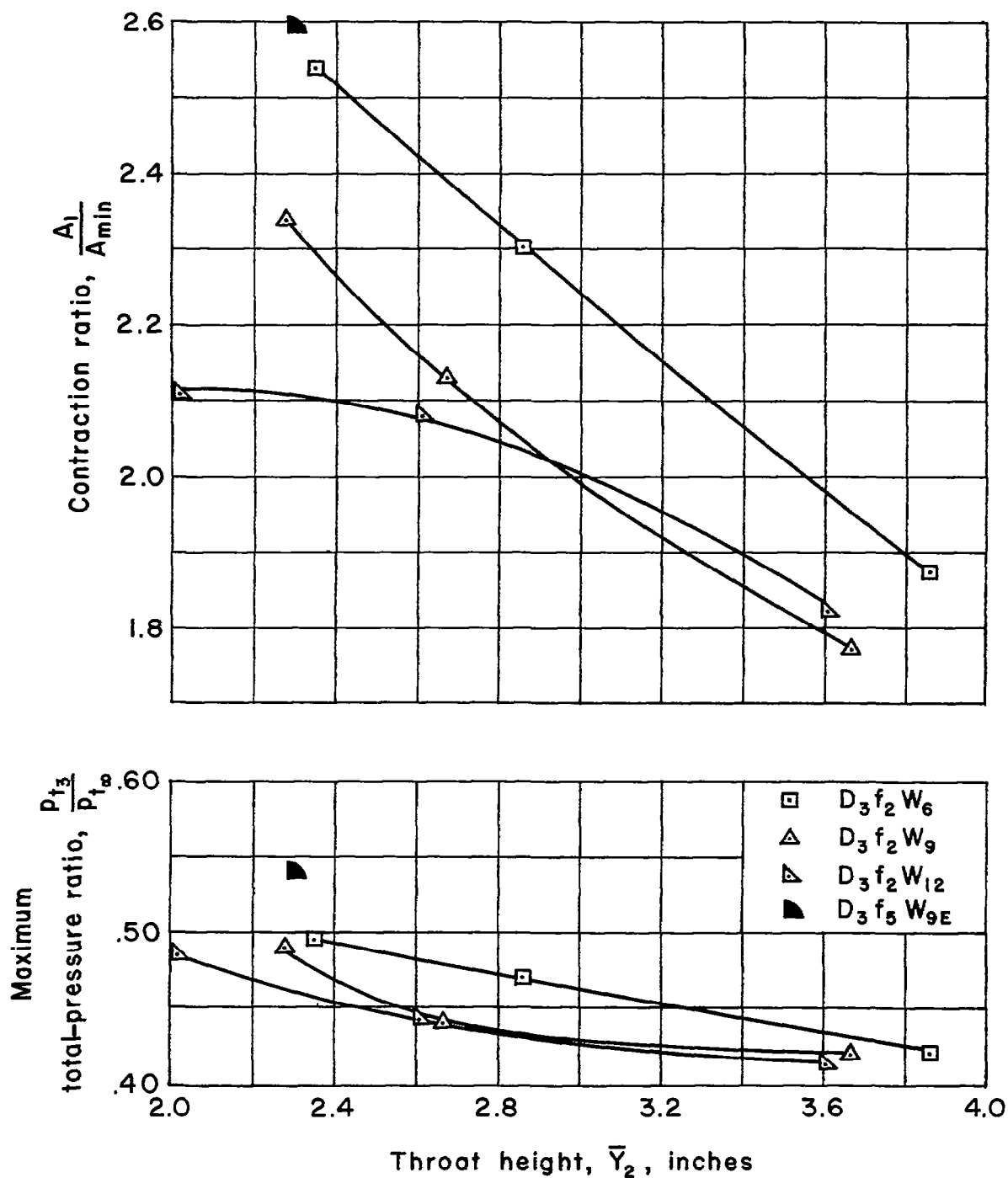


Figure 11.- Comparison of the total-pressure ratio and contraction ratios of the long and short flexure configurations with several inserts at $M_\infty = 2.92$.

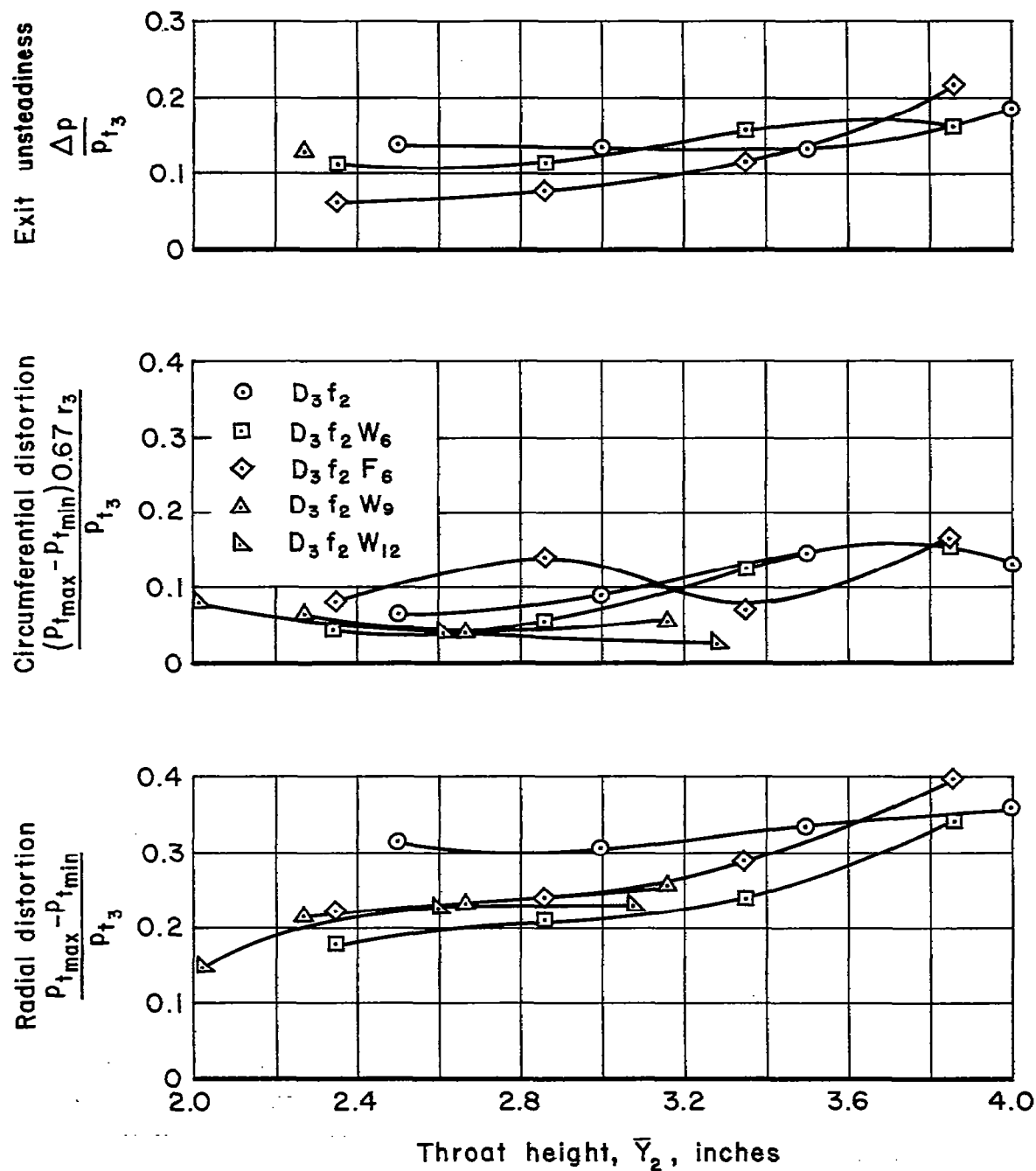


Figure 12.- Comparison of the unsteadiness and distortion with the short inserts with the short flexure at $M_\infty = 2.50$.

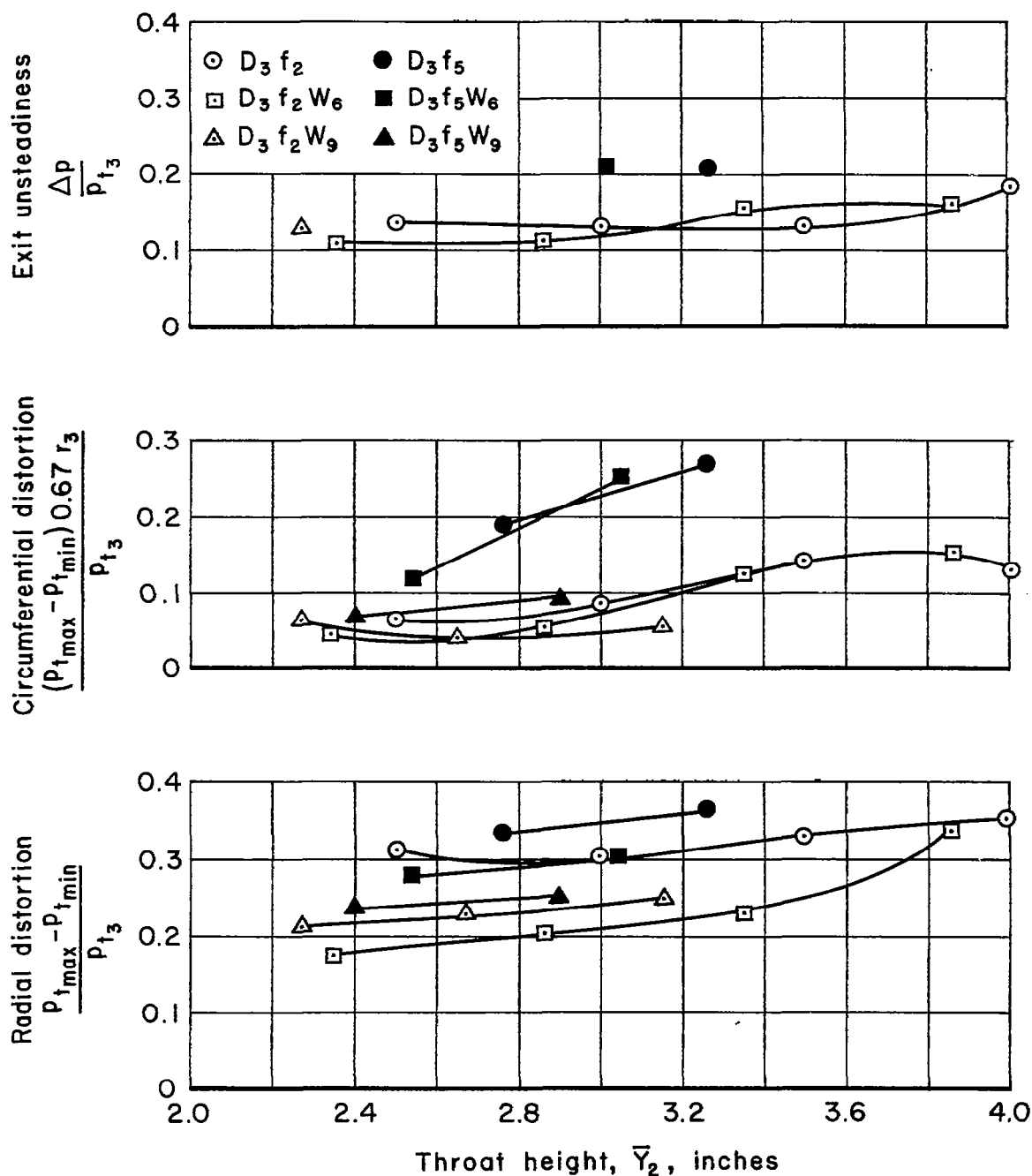


Figure 13.- Comparison of exit flow distortion and unsteadiness of the long and short flexure configurations with several inserts at $M_\infty = 2.50$.

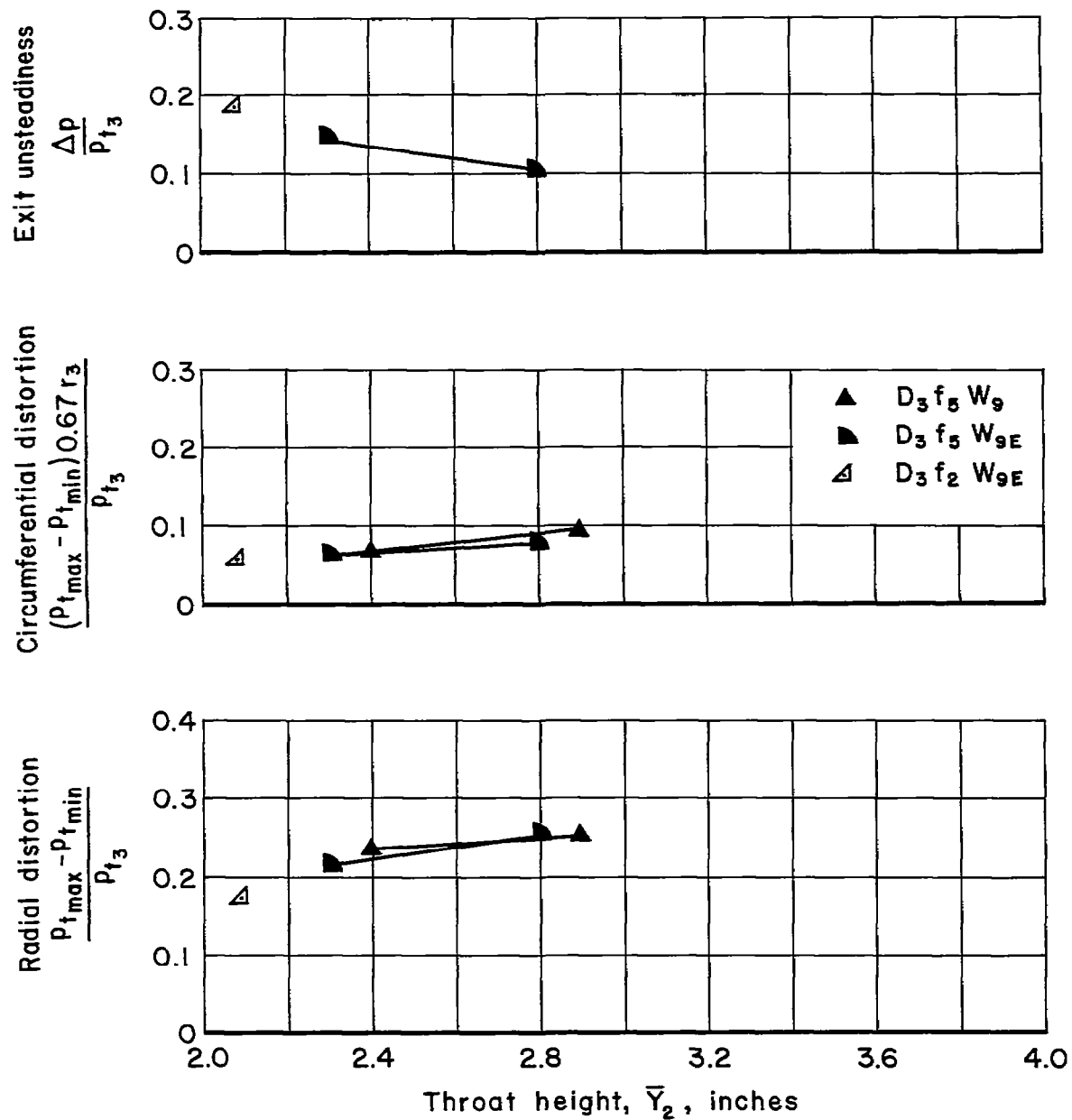


Figure 14.- Comparison of the flow distortion and unsteadiness of the extended and short 9° inserts at $M_\infty = 2.50$.

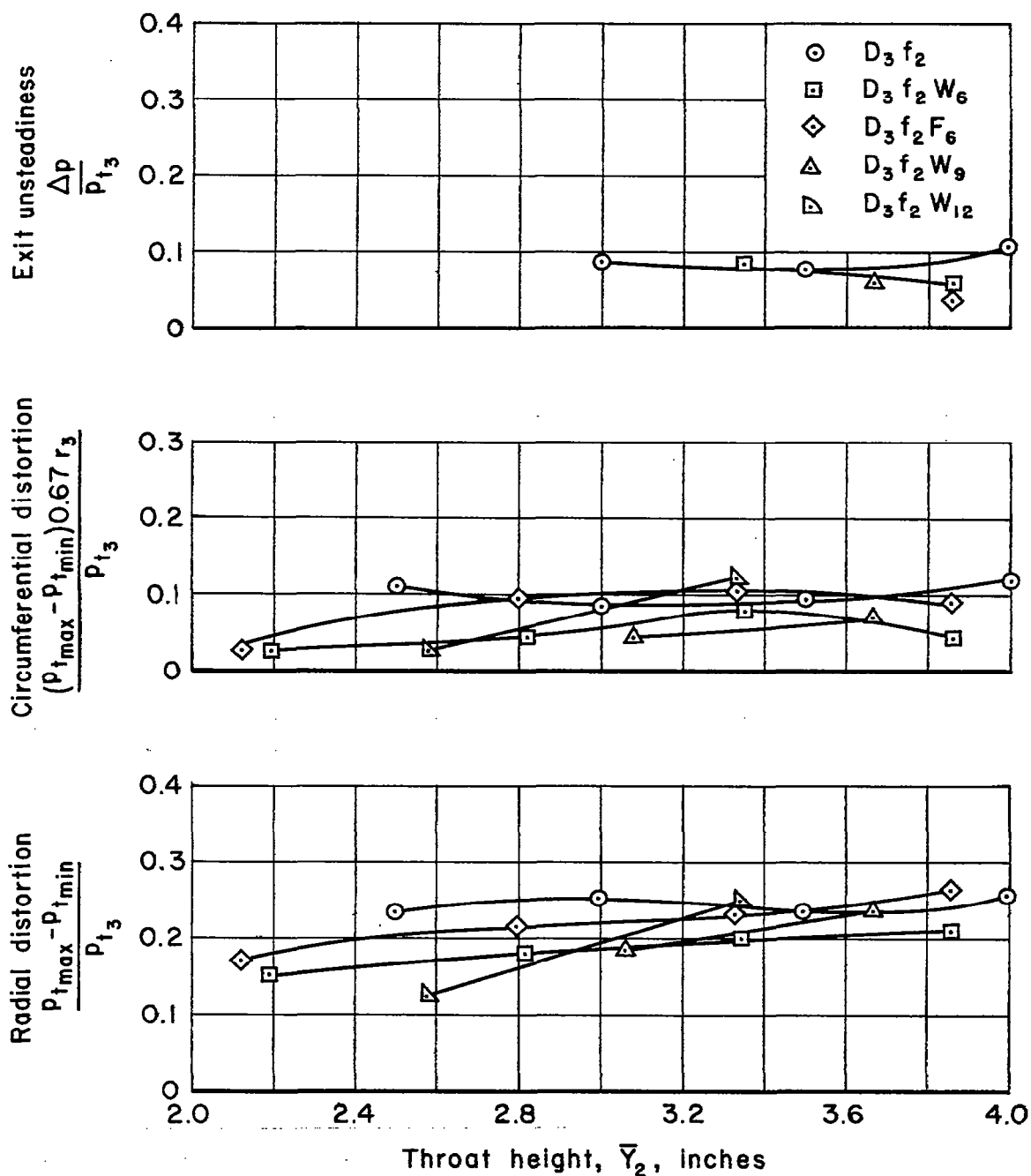


Figure 15.- Comparison of the flow distortion and unsteadiness with the short inserts with the short flexure at $M_\infty = 2.00$.

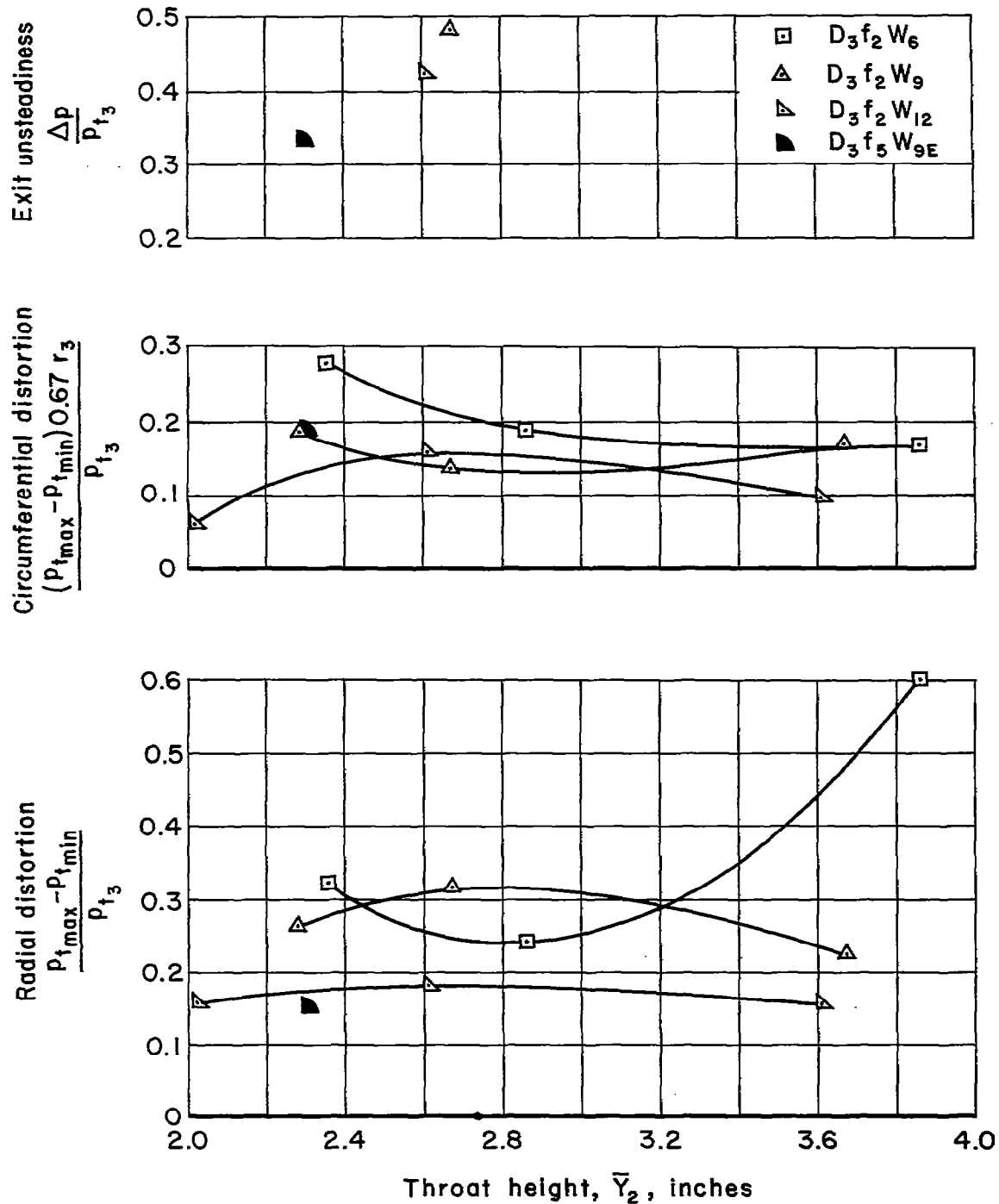


Figure 16.- Comparison of exit flow distortion and unsteadiness for the long and short flexure configurations with several inserts at $M_{\infty} = 2.92$.

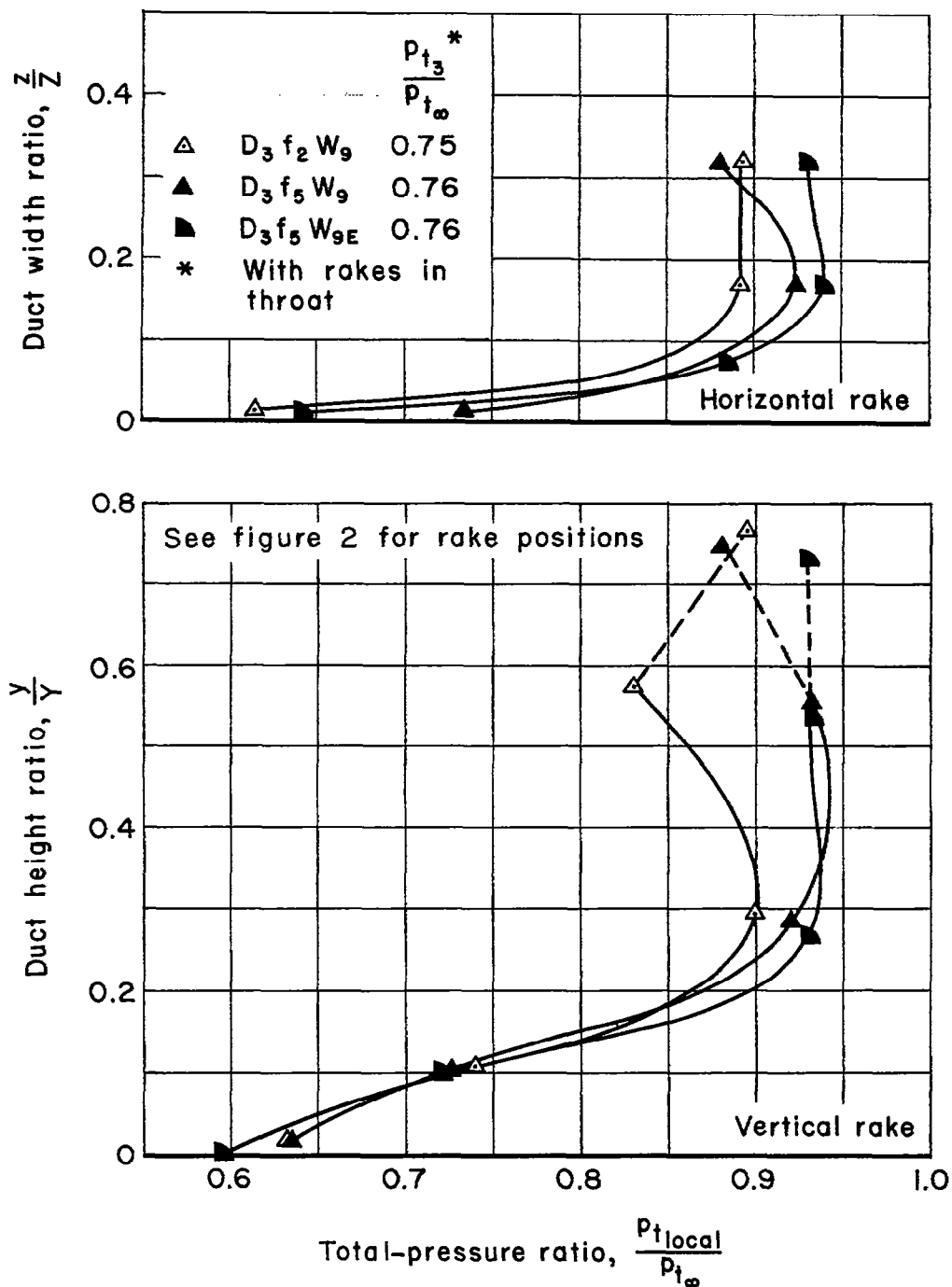


Figure 17.- Total-pressure profiles near station 17 for the three configurations having the best total-pressure recovery at $M_{\infty} = 2.50$.

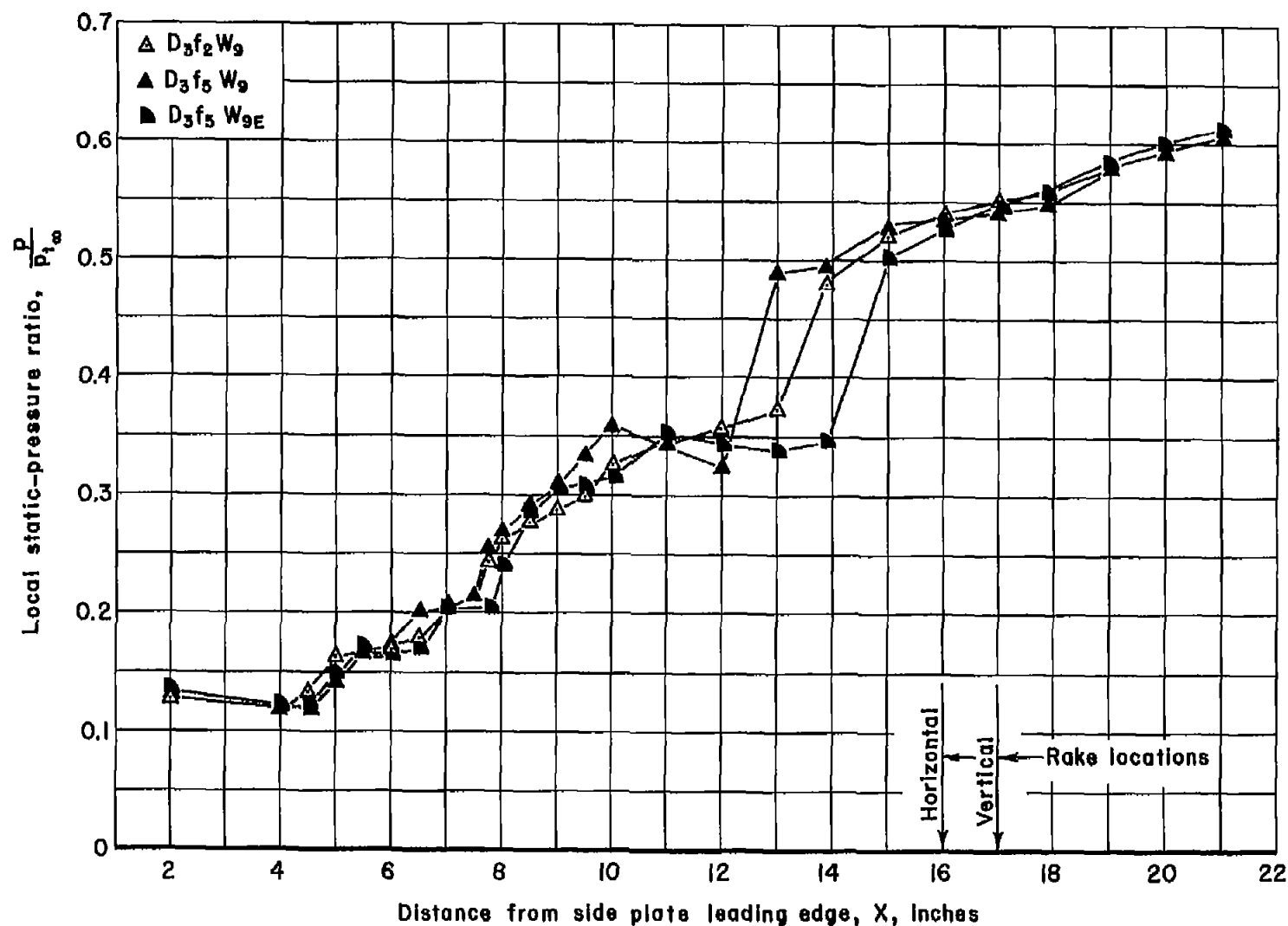


Figure 18.- Longitudinal static-pressure distributions on the side wall for the three configurations having the best total-pressure recovery; $M_\infty = 2.50$.

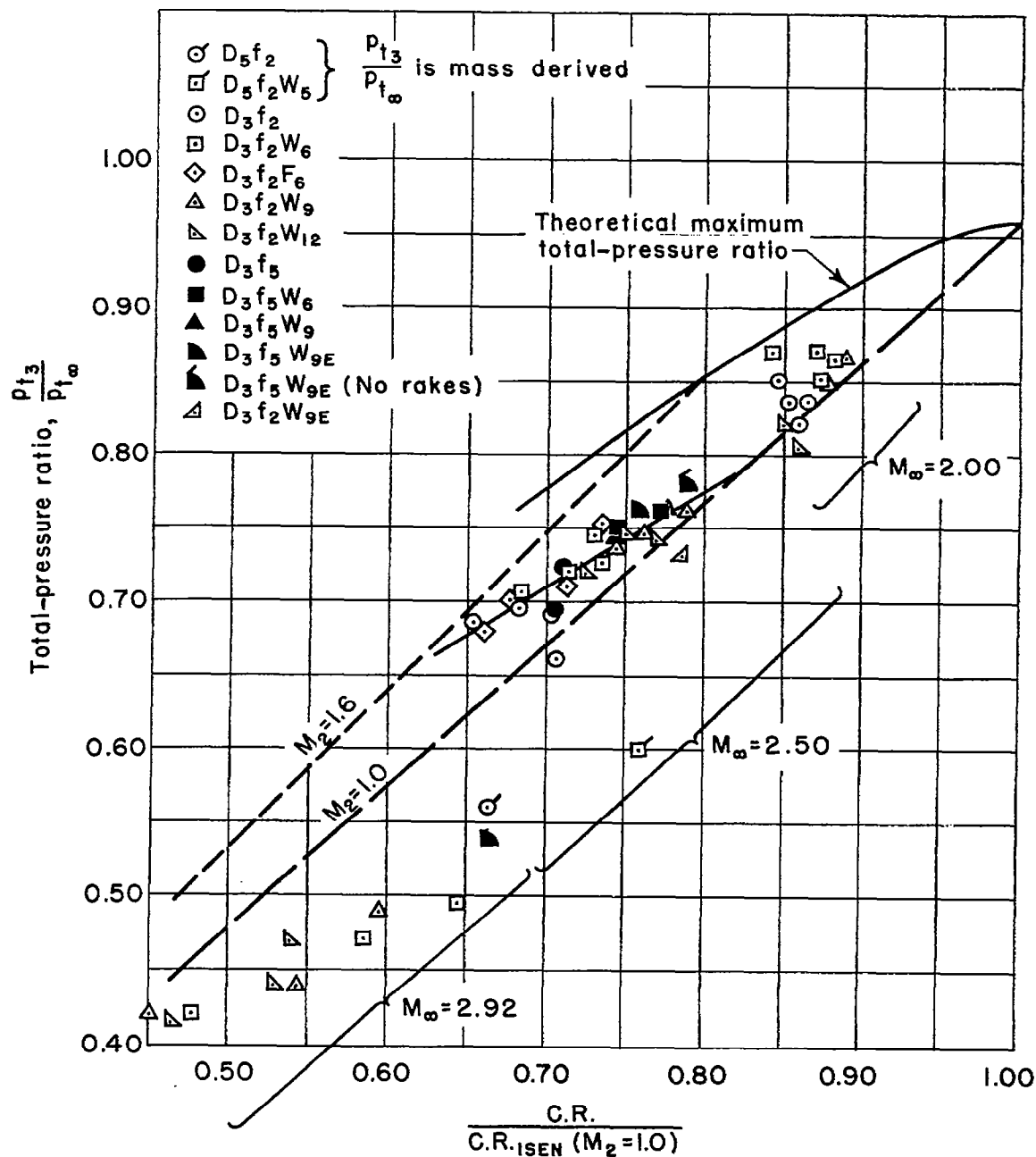


Figure 19.- Variation of total-pressure ratio with relative contraction ratio.

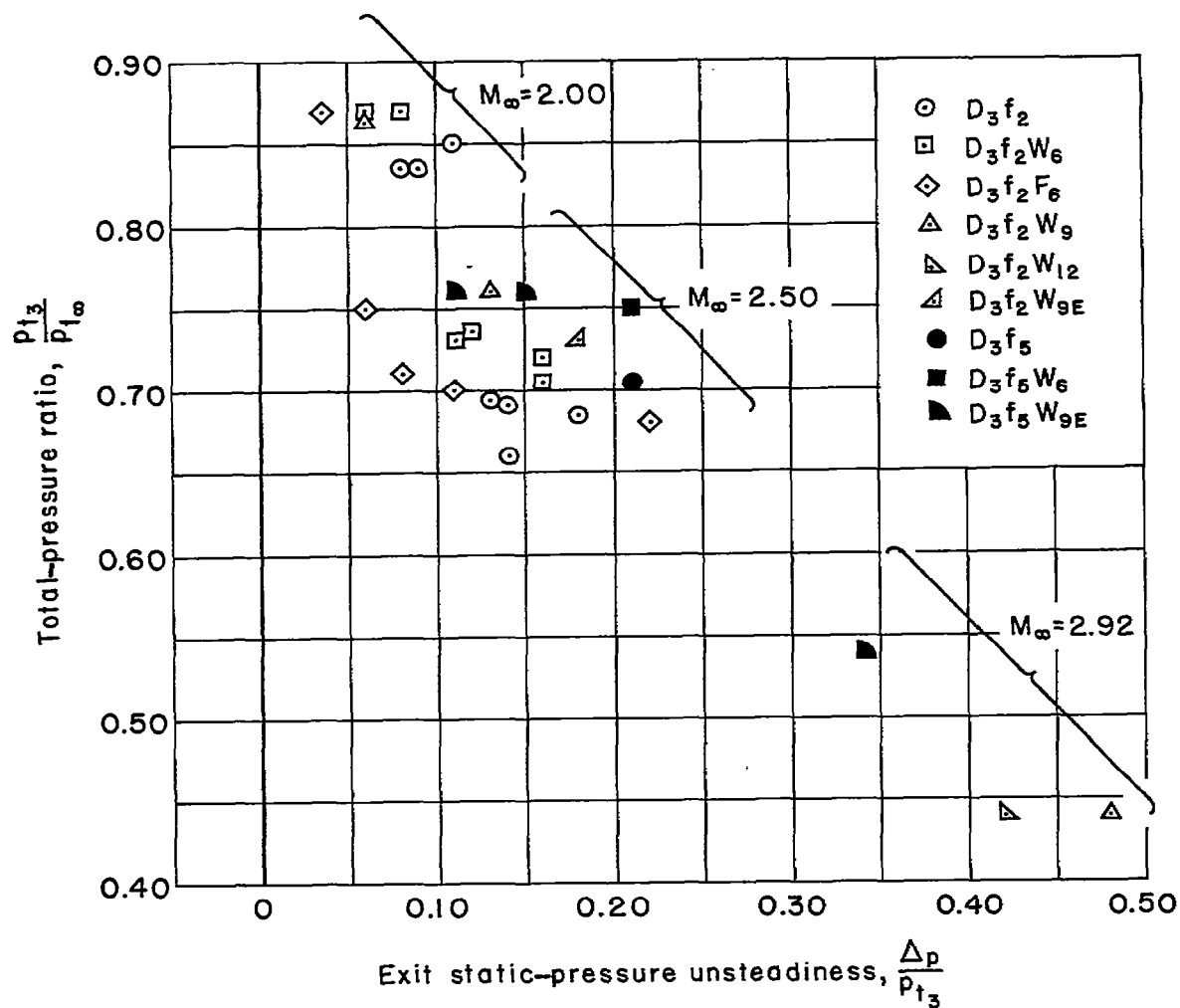


Figure 20.- Variation of total-pressure ratio with exit flow unsteadiness.

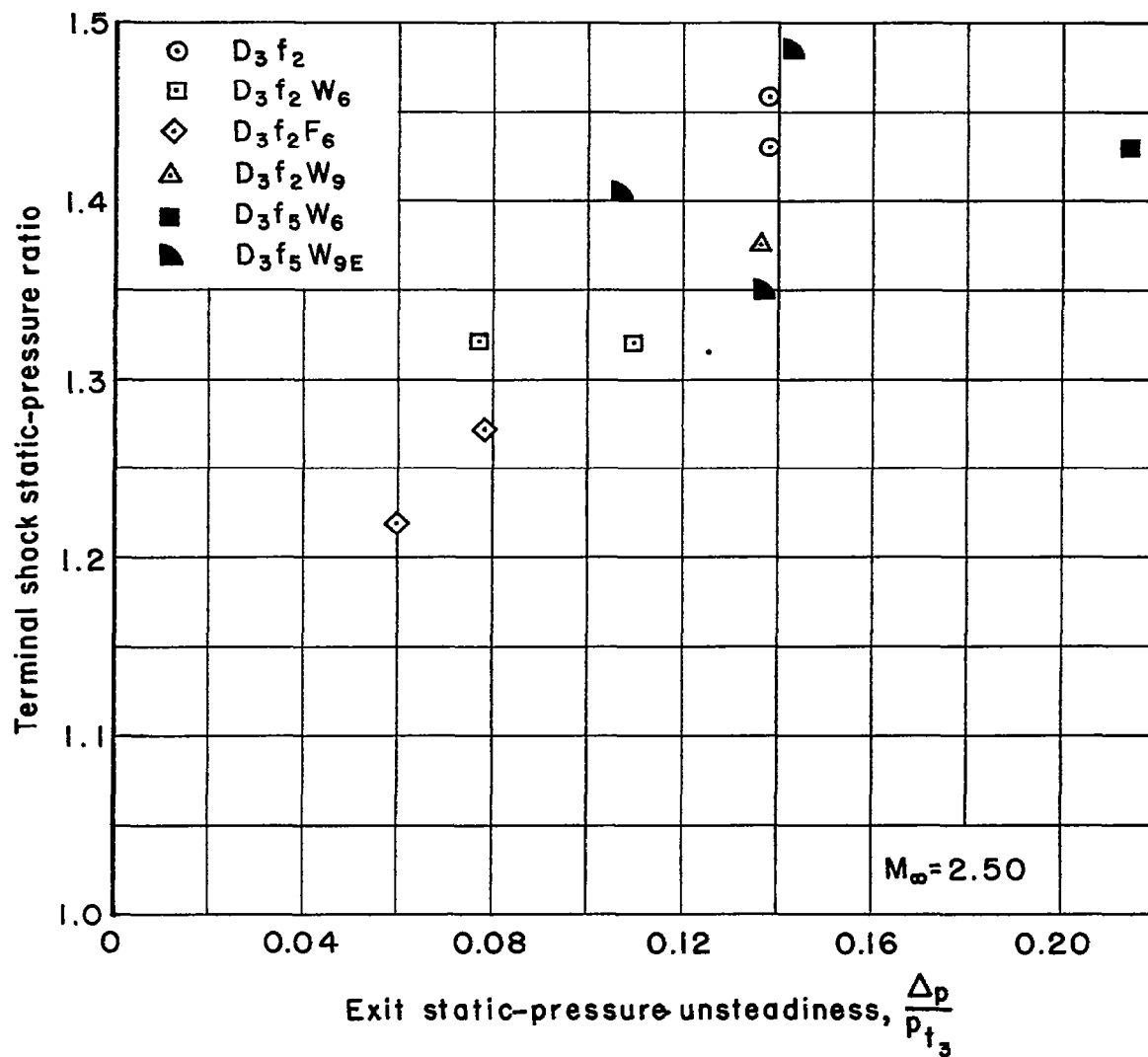
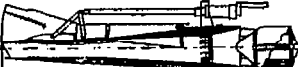
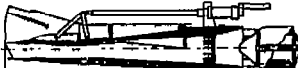
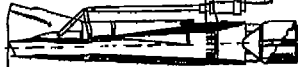


Figure 21.- Variation of terminal shock pressure ratio with exit unsteadiness.

~~CONFIDENTIAL~~

NOTES: (1) Reynolds number is based on the diameter of a circle with the same area as that of the capture area of the inlet.

(2) The symbol * denotes the occurrence of buzz.

Report and facility	Description			Test parameters				Test data				Performance		Remarks
	Configuration	Number of oblique shocks	Type of boundary-layer control	Free-stream Mach number	Reynolds number $\times 10^{-6}$	Angle of attack, deg	Angle of yaw, deg	Drag	Inlet-flow profile	Discharge-flow profile	Flow picture	Maximum total-pressure recovery	Mass-flow ratio	
RM A58024 Ames 1- by 3-foot supersonic wind tunnel		3+	None	2.0 to 2.9	3	0	0	No	Throat profile	Yes	No	0.85 at M = 2.00 0.78 at M = 2.50	1.0	
RM A58024 Ames 1- by 3-foot supersonic wind tunnel		3+	None	2.0 to 2.9	3	0	0	No	Throat profile	Yes	No	0.85 at M = 2.00 0.78 at M = 2.50	1.0	
RM A58024 Ames 1- by 3-foot supersonic wind tunnel		3+	None	2.0 to 2.9	3	0	0	No	Throat profile	Yes	No	0.85 at M = 2.00 0.78 at M = 2.50	1.0	

NASA Technical Library



3 1176 01434 9584

~~CONFIDENTIAL~~